JOURNAL OF SPACECRAFT AND ROCKETS
Vol. 32, No. 2, March–April 1995

Application of Integral Methods to Ablation Charring Erosion, A Review

Robert L. Potts*
Science Applications International Corporation, Torrance, California 90501

To predict ablation, charring, and erosion of heat-shield materials, approximate heat balance integral (HBI) methods offer speed and versatility; however, traditional HBI articles treat only simple, idealized models of material response. This paper reviews application of HBI methods to more realistic models of material response, specifically, for carbon-carbon and carbon-phenolic heat shields on reentry vehicles. The review shows that HBI successfully extends to most such simulations of ablation, charring, and erosion in hypersonic flow, but unexpected problems can crop up and trade-offs exist. Pertinent material models are also summarized, including efficient expressions that fit material thermal properties and carbon-air thermochemical ablation functions.

Nomenclature

B' = normalized mass flux (blowing driving force)
B'_c = normalized ablation rate, $\dot{m}_{ab}/g_h$
B'_g = normalized pyrolysis gas flux, $\dot{m}_{gw}/g_h$
c_p = specific heat, J/(g K)
c_{pg} = specific heat of pyrolysis gas, J/(g K)
E = activation energy, cal/mole
g_h = heat (and mass) transfer coefficient, g/(cm^2 s)
h = enthalpy, J/g
I = integral heat storage, J/cm^2
k = thermal conductivity, W/(cm K)
$\dot{m}$ = mass flux, g/(cm^2 s)
P = pressure, bar
$\dot{q}$ = heat flux, W/cm^2
$\dot{q}_{net}$ = net heat flux conducted into slab, W/cm^2
$\Re$ = universal gas constant, 1.987 cal/(mole K)
s = surface recession, cm
$\dot{s}$ = surface recession rate, cm/s
T = temperature, K
t = time in moving coordinate system, s
x = in-depth distance from initial surface, cm
z = in-depth distance from receding surface, cm
α = thermal diffusivity, cm^2/s
$\Delta h_{pyr(g)}$ = heat of pyrolysis per gas produced, J/g
δ = thermal penetration depth, cm
δ_c = effective char depth, cm
ε = emissivity
θ = heat density, J/cm^3
ρ = density, g/cm^3
σ = Stefan-Boltzmann constant, 5.670 $\times 10^{-12}$ W/(cm^2 K^4)
τ = time in stationary coordinate system, s
ϕ_{blow} = blowing correction factor
ϕ_{HAL} = heating augmentation level

Subscripts

ab = ablation
c = of char
conv = convective
cw = cold wall
eq = equilibrium
er = erosion
g = of pyrolysis gas
gw = of pyrolysis gas at the wall underside
R = reaction rate
r = recovery
ref = reference (300 K, 1 atm = 1.01325 bar)
rr = re-radiation
u = at wall underside
v = of virgin
w = at the wall (vapor-side for h_w, $\dot{m}_w$, P_w; solid-side for h_{gw}, $\dot{m}_{gw}$, θ_w, ρ_w)
0 = without blowing correction
0,0 = without blowing or heating augmentation

Superscripts

o = old
$*$ = non-dimensionalized quantity

I. Introduction

PROBLEMS of ablation, charring, and erosion of thermal protection materials in severe convective, aerothermal, often particle-laden environments have been of long and continuing interest.[1–10] Complex models and exact numerical methods abound. But even with today's computer power, the demands of some engagement studies, Monte Carlo simulations, and fully-coupled approaches preclude sole use of exact methods.[10,11] Moreover, for many concept screenings, mission analyses, and large parametric studies, fast, approximate methods are more economical.

Among fast, approximate methods, heat balance integral (HBI) methods have long been popular. Developed in the late 1950s and early 1960s, particularly by Goodman,[12] HBI methods provide simple, approximate, semi-analytical solutions to many problems of nonlinear heat transfer into solid slabs. HBI methods, in contrast to strictly analytical techniques, handle nonlinear boundary conditions, temperature-dependent properties, phase change, and moving boundaries. HBI numerical solutions usually run at least an order of magnitude faster on the computer than more exact finite-difference methods. Yet HBI solutions provide sufficient accuracy for many practical problems. Most recently, HBI has been put forth as a good way of providing dynamic boundary conditions in intensely computational fluid dynamics codes.[10]

References 12–24, and the hundred or more references these in turn cite, represent the vast HBI literature. HBI methods seem particularly applicable to ablation, charring, erosion problems, but most HBI accounts in books and journals treat only the simplest models of ablation and thermal performance; e.g., constant properties, neglect of in-depth charring, simple phase-change removal (at a known, fixed "melt" temperature), and heat loads that are either

Presented in part as Paper 90-1677 at the AIAA/ASME 5th Joint Thermophysics and Heat Transfer Conference, Seattle, WA, June 18–20, 1990 and Paper 84-0393 at the AIAA 22nd Aerospace Sciences Meeting, Reno, NV, Jan. 9–12, 1984; received Oct. 8, 1993; revision received Sept. 21, 1994; accepted for publication Sept. 28, 1994.

*Senior Scientist, 21151 Western Avenue. Member AIAA.

constant or at most simple functions of time. The special problems that arise when these idealizations no longer hold are too often ignored or handled incompletely. A need exists to bridge the gap between more realistic models of heat-shield behavior and HBI practice.

The objective of this work is to assess the extent to which HBI methods can be applied to modern, detailed, more realistic models of ablation, charring, and erosion. Using the example of carbon-carbon and carbon-phenolic heat shields on re-entry vehicles, the review shows that HBI successfully extends to most such simulations of ablation, charring, and erosion in hypersonic flow, but unexpected problems can crop up and trade-offs exist. The trade-offs involve not only speed and accuracy but also competing simplifying assumptions and solution objectives.

To satisfy the stated objective, it is necessary to establish "more realistic" material response models for consideration. In fact, to reach a wide audience, completeness and clarity dictate considerable detail, especially because of differences in notation and formulation in the literature. Accordingly, to form a consistent framework, provide necessary detail, and help set priorities for trade-offs, the first half of this paper offers appropriate illustrative models.

The second half of this paper discusses HBI methods. HBI extensions unfold as offshoots of classical theory. An example of non-charring, clear-air re-entry illustrates baseline performance of classical HBI. Modified approaches for rising and falling (pulse-like) heat loads and for charring are discussed. Note is made to Ref. 24, which develops a recent modification of HBI for variable heating and charring. Reference 24 compares its approach to finite-difference calculations[7] and to the integral-quasisteady approach[22] featured below. These comparisons support the conclusions and recommendations given below.

II. Response Models for Carbonaceous Materials

This section provides limited but sufficiently comprehensive, "more realistic" response models to study interaction with HBI methods. The models apply to general heating of slabs by hot, boundary-layer flow, but focus is on hypersonic re-entry of a blunt re-entry vehicle (RV) for illustration.

Sacrificial mass loss of heat-shield material is well established as a means of mitigating the aeroheating load for a single re-entry.[1] In this paper, ablation refers to mass loss due to thermochemical processes (e.g., melting, vaporization, oxidation, and sublimation), while erosion refers to mass loss by mechanical means, specifically, by multiple impacts of small airborne particles, such as ice crystals, snow flakes, rain drops, or even lofted dust and debris.[5–9,11]

Two heat-shield materials, a carbon-carbon and a carbon-phenolic, are of primary interest (the likeness of these materials to graphite is also exploited). The carbon-carbon consists of a three-dimensional orthogonal weave of carbon fibers with additional carbon deposited in the weave. The carbon-phenolic consists of layers of woven carbon cloth impregnated with a phenolic resin. Both materials exhibit temperature-dependent properties, and both oxidize exothermally. These traits complicate ablation calculations and produce potential difficulties for HBI methods.

The charring behavior of carbon-phenolic presents even greater challenges. At elevated temperatures, the phenolic resin decomposes in-depth, yielding pyrolysis gases that percolate to the surface and leave behind a carbon residue on the carbon cloth.[2–4] "Virgin" material thus becomes "charred." The resin decomposes mainly by endothermic chemical reactions, and the resulting pyrolysis gases absorb further heat as they percolate to the surface through porous, already charred material. Pyrolysis gases strongly affect surface thermochemistry and surface ablation rates.[25] Also, the venting of pyrolysis gases into the boundary layer blocks some of the incident heat.[2,3,15] The solid material sometimes swells, and the carbon fabric sometimes curls, lifts, and separates (delaminates), creating large gaps between the plies, thereby decreasing the conductive heat transfer.[26] Finally, although fully charred material is more fragile than virgin material, both offer non-negligible resistance to erosion.[8] Even fast-running approximate solution methods must address these issues.

In-Depth Governing Equations and Boundary Conditions

The main goal is to obtain accurate prediction of surface recession. In-depth phenomena are of interest only as they affect surface recession, but this effect is considerable.

For heat-shield configurations of interest, a one-dimensional model suffices. The classical heat conduction equation governs heat transfer in a non-charring ablator, such as carbon-carbon or graphite; thus,

$$\rho c_p \frac{\partial T}{\partial \tau} = \frac{\partial}{\partial x}\left(k\frac{\partial T}{\partial x}\right) \tag{1}$$

where the material properties c_p and k are taken as known functions of T, and material density ρ is generally constant. For a charring ablator, such as carbon-phenolic, density varies dynamically, and additional terms must be added to account for the heat absorbed in the in-depth resin breakdown and the pyrolysis gas transport to the surface. Additional equations are also required to specify conservation of mass and rate of resin decomposition. The resulting set of coupled partial differential equations takes the now customary form[2–4,7,22]

$$\rho c_p \frac{\partial T}{\partial \tau} = \frac{\partial}{\partial x}\left(k\frac{\partial T}{\partial x}\right) + \Delta h_{\mathrm{pyr}(g)}\frac{\partial \rho}{\partial \tau} + \dot{m}_g c_{\mathrm{pg}}\frac{\partial T}{\partial x} \tag{2}$$

$$\frac{\partial \dot{m}_g}{\partial x} = \frac{\partial \rho}{\partial \tau} \tag{3}$$

$$\frac{\partial \rho}{\partial \tau} = -\rho_v\left(\frac{\rho-\rho_c}{\rho_v-\rho_c}\right)^{\eta}\sum_{j=1}^{N} A_j \exp\left(\frac{-B_j}{T}\right) \tag{4}$$

Here T, ρ, and $\dot{m}_g$ are the dependent variables (unknowns) to solve for in terms of the independent variables x and τ. Following historical convention, x points into the surface, while $\dot{m}_g$ denotes gas flow out of the surface; thus, $\dot{m}_g$ is positive in the negative x direction (Fig. 1). In Eq. (4), virgin density ρ_v, fully-charred density ρ_c, reaction order η, number of legs in Arrhenius fit of char reactions N, collision frequencies $A_j[\mathrm{s}^{-1}]$, and activation temperatures $B_j = E_j/\Re$ are experimentally-known constants.[2,4,7,22,27]

References 3 and 22 derive Eqs. (2–4) from fundamental principles, state the modeling assumptions, and include historical reviews of modeling approaches. They show that heat of pyrolysis per unit mass of gas produced at the local temperature is $\Delta h_{\mathrm{pyr}(g)} = h_g - \bar{h}$ where $\bar{h} = (\rho_v h_v - \rho_c h_c)/(\rho_v - \rho_c)$ and where enthalpies of virgin, charred, and gaseous matter are each expressed as heat of formation plus integral of specific heat from reference to local temperature.[3,22] Essentially $\Delta h_{\mathrm{pyr}(g)}$ is a monotone increasing function of temperature; sometimes it is taken as a large positive constant.[7,22,27]

Thermal properties of virgin, charred, and gaseous matter differ in general. For example, the thermal conductivity of solid material in Eq. (2) is most generally a weighted value between virgin and

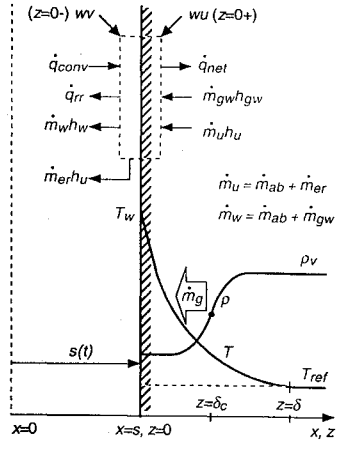

Fig. 1 Schematic of ablator material with in-depth profiles and surface energy balance.

Table 1 Carbon-carbon thermal properties

T, K	k, W/(cm K)	c_p, J/(g K)	c_p, fit[a], J/(g K)	θ[b], J/cm^3	α[b], cm^2/s
300	1.236	0.72	0.81	0	0.806
400	1.165	0.99	1.03	175	0.596
600	1.028	1.41	1.38	636	0.392
800	0.906	1.65	1.63	1210	0.293
1000	0.803	1.79	1.80	1863	0.235
1200	0.716	1.89	1.91	2569	0.197
1400	0.649	1.95	2.00	3313	0.171
1600	0.598	2.04	2.06	4084	0.153
1800	0.570	2.07	2.10	4874	0.143
2000	0.551	2.10	2.14	5680	0.136
2200	0.538	2.13	2.16	6496	0.131
2400	0.531	2.16	2.18	7322	0.128
5000	0.500	2.23	2.27	18394	0.116

[a]Equation (6).
[b]Based on c_p fit [Eq. (6)] and $\rho = 1.90$ g/cm^3.

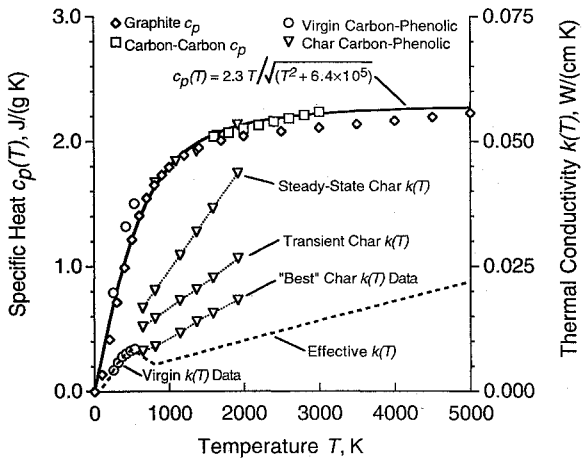

Fig. 2 Specific heat of carbonaceous materials and thermal conductivity of carbon-phenolic.

full-char limits; i.e., $\rho k = \omega\rho_v k_v + (1-\omega)\rho_c k_c$ where $\omega = (\rho - \rho_c)/(\rho_v - \rho_c)$ and where k_v and k_c are functions of temperature.[3,22] Often, however, a single, unified $k(T)$ function suffices.[22,28]

Alternative to Eq. (4), a popular simplification treats density as a function of temperature only,[3,28] or maybe char thickness as a function of time or heating rate.[3] An even simpler model converts virgin material to complete char at one particular "char temperature."[3,13] Physically, Eq. (4) may be the most realistic, but many HBI approaches require the aforementioned simplifications.

A surface energy balance furnishes the net heat flux $\dot{q}_{\text{net}}$ conducted into the solid wall. Application of Fourier's Law produces the front-face boundary condition at the moving surface

$$\left(-k\frac{\partial T}{\partial x}\right)_{x=s+} = \dot{q}_{\text{net}} \tag{5}$$

where surface recession s is determined by integrating the recession rate over time. Recession rate consists of ablation and erosion components (swelling is treated separately below); thus, $\dot{s} = \dot{s}_{\text{ab}} + \dot{s}_{\text{er}}$.

For applications of interest, either an adiabatic back wall or a semi-infinite slab assumption defines a back-face boundary condition. For initial conditions, the heat shield material begins with virgin density and stands at a cold reference temperature $T_{\text{ref}} = 300$ K.

Material Properties

Carbon-carbon thermal conductivity (Table 1) is taken from Ref. 29. Note that thermal conductivity drops sharply with temperature until it asymptotically approaches a lower bound—approximately 0.5 W/(cm K) for this particular billet. Graphite and carbon-carbons in general behave similarly.[21,30,31] Specific heat in Table 1 and Fig. 2 stems from a combination of JANAF[32] values for graphite and values reported by Ref. 33 for carbon-carbon (for the range 1600–2400 K in Table 1).

Table 2 Carbon-phenolic thermal properties

T, K	ρ, g/cm^3	c_p, J/(g K)	k, W/(cm K)	θ, J/cm^3	α, cm^2/s
300	1.45	0.94	0.0056	0	0.0041
422	1.45	1.32	0.0076	200	0.0040
533	1.45	1.51	0.0085	428	0.0039
811	1.19	1.67	0.0054	1011	0.0027
1367	1.19	1.92	0.0077	2203	0.0034
1922	1.19	2.13	0.0099	3544	0.0039
5000	1.19	2.30	0.0222	11670	0.0081

Both the surface energy balance and the HBI solution presented later require the integral of solid specific heat. Although table interpolation can be made fast in a computer code, a functional expression is convenient. In the low temperature regime (0–500 K), the specific heat of carbon-carbon and graphite is nearly linear; e.g., $c_p \approx c_1 T$. For very high temperatures, the specific heat is nearly constant, $c_p \approx C_\infty$. To develop a smooth transition between these distinct data regimes, form $(c_p)^{-2} = (c_1 T)^{-2} + (C_\infty)^{-2}$ which produces

$$c_p = C_\infty \frac{T}{\sqrt{T^2 + D^2}} \tag{6}$$

where $C_\infty = 0.55$ cal/(g K) $= 2.3$ J/(g K) and $D = C_\infty/c_1 = 800$ K. Table 1 and Fig. 2 show that Eq. (6) fits graphite,[30,32] carbon-carbon,[33] and even carbon-phenolic[27] specific heat data reasonably well over the entire domain. Unlike least-squares polynomial fits, which tend to wiggle and shoot off to infinity for large inputs, Eq. (6) remains smooth and well-behaved. Moreover, Eq. (6) integrates in closed form to

$$h_u = \int_{T_{\text{ref}}}^{T_w} c_p\,dT = C_\infty\left(\sqrt{T_w^2 + D^2} - \sqrt{T_{\text{ref}}^2 + D^2}\right) \tag{7}$$

For carbon-phenolic thermal conductivity, Fig. 2 illustrates the wide range in available values.[2,4,27] Char conductivity measurements under transient conditions fall below those of steady-state conditions. Basically, the higher the operative heat rate, the lower the char conductivity. "Best" measured and "effective" char conductivity for re-entry heat rates in Fig. 2 stem from Ref. 27 for a carbon-phenolic with cloth lay-up angle of 20 degrees.

Effective rather than measured properties are often required to achieve good correlation with flight data.[27,34] Effective values arise because thermal properties and decomposition coefficients for charring ablators are often a function of the heating rate and conditions under which they are to be used.[34] Effective char conductivities may also compensate for swelling and delamination effects. The decision whether to use effective values (e.g., Table 2) rests not with getting HBI and finite-difference solutions to agree with each other, but rather with getting them to agree with certain flight data. As for the other charring ablator coefficients in Eqs. (2) and (4), Ref. 22 presents a survey, and the values in Ref. 7 may be used for illustration for carbon-phenolic.

Surface Mass and Energy Balances

Traditional HBI articles use a simple energy balance of the form $\dot{q}_{\text{net}} = Q(t) - \dot{m}_{\text{ab}} H_{\text{ab}}$, where $Q(t)$ denotes heating load as a simple polynomial or exponential function of time, and H_{ab} is the latent heat absorbed at the surface per unit mass ablated.[12–14,16,17] Often "heat of ablation," H_{ab}, is taken as a large positive constant.[28,31] This paper, however, requires a more detailed, realistic energy balance to examine the difficulties that modern response models present to HBI.

Figure 1 includes a general surface mass and energy balance appropriate for both charring and non-charring carbonaceous materials. Ablation mechanisms include oxidation and sublimation of solid carbon but exclude melting and liquid layer formation; only a gaseous phase exists next to the solid, reacting surface. The wv- and wu-control surfaces in Fig. 1 lie infinitesimally close to the actual material surface on the wall vapor side and under side, respectively. Conservation of mass requires

$$\dot{m}_w + \dot{m}_{\text{er}} = \dot{m}_u + \dot{m}_{gw} \tag{8}$$

where $\dot{m}_w$ is the (gaseous) mass transfer rate into the boundary layer; i.e., bulk mass flux of the reacted mixture of ablation and pyrolysis gas products. The mass flux of solid material disappearing from the surface consists of thermochemical ablation and particle erosion components; i.e., $\dot{m}_u = \dot{m}_{ab} + \dot{m}_{er}$. When the latter is substituted into Eq. (8), there results $\dot{m}_w = \dot{m}_{ab} + \dot{m}_{gw}$. Conservation of energy in Fig. 1 requires

$$\dot{q}_{net} = \dot{q}_{conv} - \dot{q}_{rr} - \dot{m}_w h_w - \dot{m}_{er} h_u + \dot{m}_u h_u + \dot{m}_{gw} h_{gw} \quad (9)$$

Using $\dot{m}_u = \dot{m}_{ab} + \dot{m}_{er}$ and $\dot{m}_w = \dot{m}_{ab} + \dot{m}_{gw}$, Eq. (9) becomes

$$\dot{q}_{net} = \dot{q}_{conv} - \dot{q}_{rr} - \dot{m}_{ab}(h_w - h_u) - \dot{m}_{gw}(h_w - h_{gw}) \quad (10)$$

Following standard practice,[35,36] the convective, aerodynamic heat flux in Eq. (10) takes the form of a heat transfer coefficient g_h times enthalpy difference driving potential; i.e., $\dot{q}_{conv} = g_h(h_r - h_w)$.

Recovery enthalpy h_r is a time-dependent function of the flow, and enthalpy h_w of the gas adjacent to the wall is given below as a known function of local T_w, P_w, and possibly also $\dot{m}_{gw}$. The heat transfer coefficient already includes corrections for the effects of mass injection into the boundary layer ("blowing") and for augmented heating due to erosion-induced surface roughness and particle/flow-field interaction. Thus $g_h = g_{h0}\phi_{blow}$ and $g_{h0} = g_{h0,0}\phi_{HAL}$.

For simplicity, this paper assumes a unity Lewis number so that the mass transfer coefficient equals the heat transfer coefficient.[35] Standard, equivalent forms for correlating the blowing correction factor then are[35–37]

$$\phi_{blow} = \frac{\ln(1 + aB')}{aB'}$$
$$B' = \frac{\dot{m}_w}{g_h} = \frac{\dot{m}_{ab} + \dot{m}_{gw}}{g_h} = B'_c + B'_g \quad (11)$$

$$\phi_{blow} = \frac{aB'_0}{\exp(aB'_0) - 1}$$
$$B'_0 = \frac{\dot{m}_w}{g_{h0}} = \frac{\dot{m}_{ab} + \dot{m}_{gw}}{g_{h0}} = B'_{c0} + B'_{g0} \quad (12)$$

Substitution of $g_h = g_{h0}\phi_{blow}$ into $B' = \dot{m}_w/g_h$ shows $B' = B'_0/\phi_{blow}$. Substitution of $B' = B'_0/\phi_{blow}$ into $\phi_{blow} = \ln(1 + aB')/(aB')$ produces Eq. (12), which shows that Eqs. (11) and (12) are indeed equivalent. Both forms are required in the ablation model presented below.

The blowing coefficient a in Eqs. (11) and (12) varies in general with injectant gas species, flow conditions (stagnation point, laminar, or turbulent), and Mach number.[35] For illustration, however, constants $a = 1.5$ for carbon-carbon and $a = 1.3$ for carbon-phenolic have been selected based on the data in Fig. 4 of Ref. 37.

The heating augmentation level ($\phi_{HAL} \geq 1$) is obtained from the theory of Hove-Shih.[38] For clear air flight, assume $\phi_{HAL} = 1$.

The reference point for all enthalpies in this paper is T_{ref}, so $h_w = 0$ for a cold, non-ablating wall in air. Then the aeroheating history may be expressed by way of a "cold wall" heat flux, defined $\dot{q}_{cw} = g_{h0,0}h_r$.

Local pressure is assumed constant across the thin boundary layer from outer edge to wall; i.e., $P_e = P_w = P$. Local P, h_r, and $\dot{q}_{cw}$ or $g_{h0,0}$ are time-dependent and available from standard aerodynamic flow and boundary layer calculations.[35]

Following another common practice, and using $\varepsilon = 0.90$ for carbon-carbon[21,30] and $\varepsilon = 0.85$ for carbon-phenolic,[27] the net heat flux re-radiated from the surface is modeled as $\dot{q}_{rr} = \varepsilon\sigma(T_w^4 - T_{ref}^4)$.

Note back in Eq. (10) that the erosion mass flux dropped out. The reason is that eroded material does not change phase between the wu and wv surfaces. Even so, erosion significantly affects the surface energy balance. Specifically, increased erosion lowers T_w, which usually lowers h_w and thus raises $\dot{q}_{conv} = g_h(h_r - h_w)$. Also, erosive environments lead to heating augmentation,which raises g_h and thus $\dot{q}_{conv}$.

Sometimes, to simplify matters, the pyrolysis gases are assumed chemically inert with respect to the boundary layer gases (Ref. 35, p. 65). In that case the $\dot{m}_{gw}$ terms drop out of the Eq. (10) energy balance in the same way that $\dot{m}_{er}$ terms dropped out (e.g., replace $\dot{m}_w h_w$ in Fig. 1 with $\dot{m}_{ab}h_w + \dot{m}_{gw}h_{gw}$). The end result is the energy balance used in this paper:

$$\dot{q}_{net} = \dot{q}_{cw}(1 - h_w/h_r)\phi_{HAL}\phi_{blow} - \varepsilon\sigma\left(T_w^4 - T_{ref}^4\right) - \dot{m}_{ab}(h_w - h_u) \quad (13)$$

Ablation Model

Traditional HBI articles model ablation as melting of a solid with complete, instantaneous removal of melt (e.g., by aerodynamic shear).[12–14,16,17] In a preablation period, the surface heats up to the fixed, known, melt or ablation temperature. There follows an ablation (melt removal) period, in which the ablation rate (rather than wall temperature) is the unknown to solve for. For carbon oxidation and sublimation, however, more realistic models than "removal of melt" exist, and the difficulties that such models present to HBI methods deserve treatment.

Chemical equilibrium has become a standard assumption for computing re-entry vehicle and rocket nozzle ablation.[3,10,25,30,35,39] The idea is that significant heating and ablation occur mainly in a regime where boundary layer temperatures and pressures are high enough for reactions to be very fast and for chemical equilibrium to prevail. Equilibrium surface thermochemistry (EST) calculations are made for an open system comprised of the boundary-layer gas mixture adjacent to the ablating carbon surface. The pertinent mass fluxes (mass crosses open-system boundaries) are boundary-layer flow past the wall (convection), diffusion of air constituents (especially O_2) into and through the boundary layer, ablation of carbon surface material, and, for carbon-phenolic, injection of pyrolysis gases. Only relative amounts of chemical elements are required to compute equilibrium. Thus, it suffices to specify B'_c, B'_g, system pressure P, and the elemental compositions of air, pyrolysis gas, and the surface (100% solid carbon). Given prescribed values of these quantities, the equilibrium composition, temperature, and enthalpy of the open system (wall gas mixture) are calculated. This process is repeated for a large matrix of (B'_c, B'_g, P) conditions. To compute ablation rates, the resultant table of EST calculations is interpolated: given T_w, P, and B'_g, find B'_c and h_w.

Figure 3 shows calculations for carbon ablation in air made using a standard EST computer code.[40] Thermodynamic inputs to the code stem mainly from the data for C-N-O species in the JANAF thermodynamic database,[32] controversies notwithstanding[41] (Ref. 21 provides more details). At temperatures greater than 1500 K, all the oxygen diffusing through the boundary layer is consumed in the reaction at the wall. This limits the reaction rate and produces the flat B'_c plateau in Fig. 3. Assuming a freestream composition of 23.2% O_2 and 76.8% N_2 by mass, and a single oxidation reaction of complete CO formation, theory[35] shows $B'_c = 0.174$ (= 12/16 of 0.232), and the gas composition at the wall is 65.4% N_2 (= 0.768/1.174) and 34.6% CO. At higher temperatures, sublimation of carbon occurs, producing sharp, pressure-dependent rises in Fig. 3. Products with high heats of formation such as CN and C_3 appear.[30,35,39]

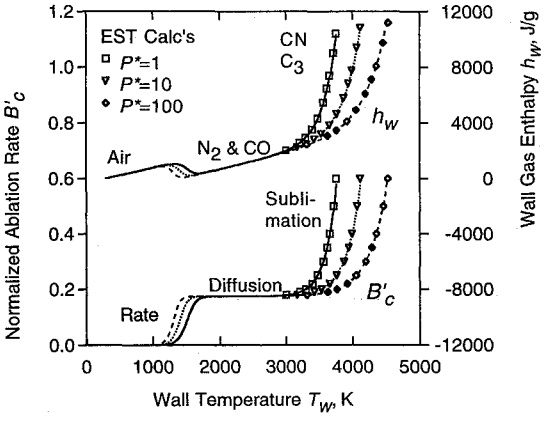

Fig. 3 Model for carbon ablation in air.

For convenience, simple equations were developed to fit the carbon-air EST calculations.[21,22] As shown in Fig. 3, the calculational data are well-fit by the general forms

$$B'_{c,\mathrm{eq}} = B'_{\mathrm{DCO}} + B'_{\mathrm{DCO}} \exp(T^*), \qquad T^* = (T_w - T_P)/S_P$$
$$T_P = (T_1)(P^*)^{q_1}, \qquad S_P = (T_2)(P^*)^{q_2}, \qquad P^* = P/P_{\mathrm{ref}} \tag{14}$$

$$h_{w,\mathrm{eq}} = \bar{h}_f + \bar{c}_p(T_w - T_{\mathrm{ref}}) + h'_S(B'_{c,\mathrm{eq}} - B'_{\mathrm{DCO}})^{q_3} \tag{15}$$

where $P_{\mathrm{ref}} = 1$ atm $= 1.01325$ bar. In Eq. (14), T_P and S_P locate and scale, respectively, the steep sublimation rise above the diffusion-controlled oxidation (DCO) plateau $B'_{\mathrm{DCO}} = 0.174$. Best-fit constants are $T_1 = 6510°\mathrm{R} = 3616.\bar{6}$ K, $q_1 = 0.0367$, $T_2 = 305°\mathrm{R} = 169.\bar{4}$ K, and $q_2 = 0.104$. In Eq. (15), best-fit constants are $\bar{h}_f = -587$ Btu/lbm $= -1365$ J/g (heat of formation of 34.6% CO), $\bar{c}_p = 0.282$ Btu/(lbm°R) $= 1.18$ J/(g K), $h'_S = 7000$ Btu/lbm $= 16280$ J/g, and $q_3 = 0.845$ for the JANAF reference temperature 25°C $= 298.15$ K ($\approx T_{\mathrm{ref}} = 300$ K).

Note in Fig. 3 that the sublimation regime shifts horizontally with $\log P^*$. Also, $(P^*)^q = \exp\{q \log_e P^*\} = 1 + q \log_e P^* + \cdots$ in Eq. (14). Actually, for a given $\log P^*$ increment, the shift is slightly greater to the right than to the left, and the width of the B' rise increases with higher P^*, but these are nicely handled by Eq. (14).

The above model describes graphite and carbon-carbon equilibrium ablation in air. It also applies to carbon-phenolic if pyrolysis gases are inert. In the most general case, pyrolysis gases react with surface carbon and ablation products, causing shifts in the B'_c and h_w curves (see, for example, Fig. 3 of Ref. 25 and Fig. B-1 of Ref. 22). Descriptive equations that fit general carbon-phenolic-air ablation functions with reacting gas effects are available[22]; however, such complexities add little to illustrating the complications that arise with HBI. Therefore, this paper uses the inert pyrolysis gas assumption cited earlier with Eq. (13). Although B'_g fails to affect B'_c under an inert gas assumption, B'_g significantly affects both the energy balance and the ablation rate ($\dot{m}_{\mathrm{ab}} = B'_c g_h$) through the blowing correction on g_h, per Eqs. (11) and (12).

In the lowest ablating temperature range, non-equilibrium reaction rates apply. Several expressions for rate-controlled oxidation of carbonaceous materials are available.[39,41–43] For illustration, take

$$\dot{m}_R = a_R\left(X_{O_2} P^*\right)^{0.5} \exp\{-E_R/(\Re T_w)\} \tag{16}$$

from Ref. 42, where $a_R = 9.65 \times 10^5$ lbm/(ft^2 sec) $= 4.71 \times 10^5$ g/(cm^2 s), $X_{O_2} = 0.21$ = mole fraction (partial pressure) of oxygen in air, and $E_R = 44 \times 10^3$ cal/mole. Scala's second-order transition scheme[39,42] combines the rate-controlled and equilibrium expressions into an overall ablation rate; i.e.,

$$\frac{1}{\dot{m}^2_{\mathrm{ab}}} = \frac{1}{\dot{m}^2_R} + \frac{1}{\dot{m}^2_{\mathrm{eq}}} \tag{17}$$

where $\dot{m}_{\mathrm{eq}}$ is defined from $B'_{c,\mathrm{eq}}$. Note that the smaller of the $\dot{m}$'s dominates the right side of Eq. (17), so that for very high reaction rates, equilibrium prevails.

Equation (17) defines a smooth transition from rate-controlled oxidation to equilibrium oxidation according to a transition factor

$$\dot{m}_{\mathrm{ab}} = \dot{m}_{\mathrm{eq}} f_{\mathrm{tr}}, \qquad f_{\mathrm{tr}} = 1\Big/\sqrt{1 + (\dot{m}_{\mathrm{eq}}/\dot{m}_R)^2} \tag{18}$$

Note that f_{tr} approaches zero for small reaction rates and one for large reaction rates. This transition factor also defines the transition of wall gas enthalpy from air-composition based to oxidation-products based; namely,

$$h_w = f_{\mathrm{tr}} h_{w,\mathrm{eq}} + (1 - f_{\mathrm{tr}}) h_{w0}, \qquad h_{w0} = \int_{T_{\mathrm{ref}}}^{T_w} c_{p0}\, dT \tag{19}$$

where $c_{p0} = C_0 + D_0 T$ with $C_0 = 0.234$ Btu/(lbm°R) $= 0.979$ J/(g K) and $D_0 = 2 \times 10^{-5}$ Btu/(lbm°R^2) $= 1.5 \times 10^{-4}$ J/(g K^2) is the specific heat of air (Ref. 35, p. 177).

The overall sequence for energy balance calculations is now this. At a given time point, h_r, P, $\dot{q}_{\mathrm{cw}}$, and ϕ_{HAL} are available from the aerodynamic heating solution; these give $g_{h0} = (\dot{q}_{\mathrm{cw}}/h_r)\phi_{\mathrm{HAL}}$. Also available are the current guess for T_w and values $\dot{m}^o_{gw}$ and $\dot{m}^o_{\mathrm{ab}}$ from the prior time point. Charring ablator calculations require an immediate estimate of B'_g; for example, $\hat{B}'_0 = (\dot{m}^o_{\mathrm{ab}} + \dot{m}^o_{gw})/g_{h0}$, then $\hat{\phi}_{\mathrm{blow}} = a\hat{B}'_0/[\exp(a\hat{B}'_0) - 1]$ per Eq. (12), and finally $\hat{B}'_g = \dot{m}^o_{gw}/(g_{h0}\hat{\phi}_{\mathrm{blow}})$. Next $B'_{c,\mathrm{eq}}$ and $h_{w,\mathrm{eq}}$ are calculated. For carbon-phenolic with reacting pyrolysis gas, $B'_{c,\mathrm{eq}}$ and $h_{w,\mathrm{eq}}$ are functions of T_w, P, and $B'_g = \hat{B}'_g$, as shown in Ref. 22. But for carbon-carbon, graphite, and carbon-phenolic with inert pyrolysis gas, $B'_{c,\mathrm{eq}}$ and $h_{w,\mathrm{eq}}$ are simply functions of T_w and P per Eqs. (14) and (15). Equilibrium blowing conforms to Eq. (11). Note especially that both inert and reacting pyrolysis gas cases require $\hat{B}'_g$ here; i.e., first $B'_{\mathrm{eq}} = B'_{c,\mathrm{eq}} + \hat{B}'_g$, then $\phi_{\mathrm{blow,eq}} = \ln(1 + aB'_{\mathrm{eq}})/(aB'_{\mathrm{eq}})$ per Eq. (11), and finally $\dot{m}_{\mathrm{eq}} = g_{h0}\phi_{\mathrm{blow,eq}} B'_{c,\mathrm{eq}}$. Of course for non-charring ablators, $B'_g = \hat{B}'_g = 0$ always. Next, Eqs. (16–19) couple in reaction rate kinetics, which produce the ultimate $\dot{m}_{\mathrm{ab}}$ and h_w for this T_w iterate. Using this new $\dot{m}_{\mathrm{ab}}$, the blowing factor is updated via Eq. (12). This updated blowing factor is used in Eq. (13), which defines net heat flux. Note how both forms of blowing, Eqs. (11) and (12), are required in the above sequence. Finally, the ablation recession rate for heat-shield surface density ρ_w is $\dot{s}_{\mathrm{ab}} = \dot{m}_{\mathrm{ab}}/\rho_w$.

Erosion, Swelling, and Spallation

These topics are introduced to underscore the need for satisfactory prediction of certain variables. Also, certain aspects of erosion deserve mention in the open literature.

A dimensionless mass loss ratio G relates the rate of erosive mass loss to the mass flux of incident particles.[7,8,21,44,45] Generally, the mass loss ratio G (mass out over mass in) is defined empirically for each particular heat shield material. It varies roughly proportionally with particle material density and the square of the normal component of impact velocity. It also depends in general on the temperature of the heat-shield material eroded. Thus, wall temperature, near surface temperature gradient, and particle penetration depth (which depends on both the particle diameter and the extent of existing subsurface damage in the target material) come into play.

Char state also affects G. Fully charred carbon-phenolic material is more fragile than virgin material, yet both offer non-negligible resistance to erosion.[8] To account for the interplay between the transient depth of the material char layer and the particle penetration (cratering) depth, a transition-state model dynamically bridges between limiting virgin and fully-charred erosion states.[7] The model effectively produces average values $\bar{G}$ (called G_{eff} in Ref. 7) and $\bar{\rho}$ (average density of heat-shield material eroded) at each time point. The weighting factor for averaging between limiting states is essentially the ratio of char depth to effective particle penetration depth (see Ref. 7 for details). If $\dot{m}_p$ is the component of incident particle mass flux normal to the surface, the erosion recession rate is then $\dot{s}_{\mathrm{er}} = \dot{m}_{\mathrm{er}}/\bar{\rho} = \bar{G}\dot{m}_p/\bar{\rho}$.

Yet another integral averaging process arises when the RV encounters a distribution of particle sizes and types (dust, ice, rain, snow). Each class (size and type) of particle penetrates the char layer to differing depths, and each class experiences differing degrees of deceleration, deflection, and breakup in the bow shock layer surrounding the RV.[44–46] Typically, incident particle velocities, mass fluxes, $\bar{G}$, and $\bar{\rho}$ are computed for each class of particle separately, and then the class erosion recession rates are summed at each time point to get the net $\dot{s}_{\mathrm{er}}$.

Because of limited space and technology restrictions, further details are omitted. But a proper framework for erosion has been established. Besides treatment of $\dot{m}_{\mathrm{er}}$ and $g_{h0} = g_{h0,0}\phi_{\mathrm{HAL}}$ in the energy balance earlier, the discussion of G above shows that accurate erosion calculations require accurate estimates of transient wall temperature, wall temperature gradient (i.e., net heat flux), and, for carbon-phenolic, char depth. Here Ref. 7 shows that erosion and transient char formation are strongly coupled in a self-limiting process: increased char formation causes higher erosion rates, and increased erosion rates cause decreased char formation. Therefore, while transient char depth calculations cannot be passed over, approximate calculations should suffice.

Material swelling[26,47] and spallation[4,47] likewise depend on good estimates of char depth, gas flux, and near surface temperature field. For example, swelling is typically assumed roughly proportional to either pyrolysis gas flux[26] or char thickness.[47] In some approaches,[26] material swelling adds a negative recession term to overall recession rate and adds auxiliary convective terms to Eq. (2). Alternatively, this paper assumes that swelling at most modifies (decreases) effective thermal conductivity (as a pre-calculation adjustment) and stretches the in-depth scale or thermal penetration depth (as a post-calculation correction) relative to the ablating surface. Swelling in the face of erosion is unknown. In any case, the importance of obtaining good estimates of char depth and gas flux, even in an approximate solution, is again underscored.

III. Heat Balance Integral (HBI) Methods

The idea of the heat balance integral (HBI) method is to integrate the heat conduction equation spatially and then assume a profile shape for the spatial heat distribution. The original nonlinear boundary value problem (partial differential equation) reduces to a much simpler initial value problem (one or more ordinary differential equations, ODEs). The number of equations corresponds to the number of profile parameters to solve for.

From the previous section, good prediction of surface recession (primary objective) requires good prediction of wall temperature and net heat flux for all materials, and also pyrolysis gas flux and char depth for charring materials.

In order to handle temperature dependent thermal properties, it helps to convert temperature T to a thermal or heat density θ using Goodman's transformation[12]

$$\theta = \int_{T_{\text{ref}}}^{T} \rho(\tilde{T}) c_p(\tilde{T})\, \mathrm{d}\tilde{T} \tag{20}$$

Inclusion of material density inside the integral enhances the generality of Eq. (20) but imposes a simplifying restriction on charring ablators.

With Eq. (20), and with $z = x - s(\tau)$ and $t = \tau$ to transform to a coordinate system moving with the surface (differentiation by τ holds x fixed; by t, z fixed), Eqs. (1–3) and (5) assume the form

$$\frac{\partial \theta}{\partial t} = \frac{\partial}{\partial z}\left(\alpha \frac{\partial \theta}{\partial z}\right) + \dot{s}\frac{\partial \theta}{\partial z} \tag{21}$$

$$\frac{\partial \theta}{\partial t} = \frac{\partial}{\partial z}\left(\alpha \frac{\partial \theta}{\partial z}\right) + \dot{s}\frac{\partial \theta}{\partial z} + \Delta h_{\text{pyr}(g)}\frac{\partial \dot{m}_g}{\partial z} + \dot{m}_g c_{\text{pg}}\frac{\partial T}{\partial z} \tag{22}$$

$$\frac{\partial \dot{m}_g}{\partial z} = \frac{\partial \rho}{\partial t} - \dot{s}\frac{\partial \rho}{\partial z} \tag{23}$$

$$\dot{q}_{\text{net}} = \left(-\alpha \frac{\partial \theta}{\partial z}\right)_{z=0+} \tag{24}$$

As explained later under charring ablators, Eq. (4) and the final T in Eq. (22) are left as is. Thermal diffusivity $\alpha = k/(\rho c_p)$ becomes a known function of θ.

Classical HBI

For the first major step of heat balance integration (HBI), integrate the conduction equation spatially. This paper assumes a semi-infinite slab of material (Ref. 24 treats the finite slab case). Spatial integration of Eq. (21) produces

$$\frac{\mathrm{d}}{\mathrm{d}t}\int_0^\infty \theta \mathrm{d}z = \dot{q}_{\text{net}} - \theta_w \dot{s} \tag{25}$$

where Eq. (24) was applied at $z = 0$, and $\theta = 0$ and $\partial\theta/\partial z = 0$ are assumed at $z = \infty$. Equation (25) is called the heat balance integral (HBI) and is interpreted as a balance between the rate of change of heat stored in the slab per unit surface area [left side of Eq. (25)] with the rate of change of heat entering the slab surface, properly accounting for recession [right side of Eq. (25)]. Thus, the HBI is a global conservation of energy. With reference to Fig. 1, the surface energy balance is a balance between the *wv* and *wu* surfaces, and the HBI is a balance across the *wu* surface, extending at least as far as the thermal penetration in-depth.

For the second major step of HBI, assume a heat density profile shape. For constant surface heating of a semi-infinite slab at uniform initial temperature, the assumed profile is written most generally as

$$\theta(z, t) = \theta_w(t)\theta^*(z^*), \qquad z^* = z/\delta(t) \tag{26}$$

where specification of the function $\theta^*(z^*)$ fixes the profile shape. Typical choices are exponentials, $\theta^*(z^*) = \exp(-z^*)$, and n-th degree polynomials, $\theta^*(z^*) = (1 - z^*)^n$ for $0 \le z^* \le 1$ and $= 0$ for $z^* > 1$, where n need not be an integer but any real number > 1.

From Eq. (26), the heat density profile has two degrees of freedom corresponding to the two equations, Eqs. (24) and (25), in the two unknowns, $\delta(t)$ and $\theta_w(t)$. Strict use of Eq. (24) to determine the profile slope at the wall, and derivation of Eq. (25) from Eq. (21) rather than Eq. (22), distinguishes classical HBI from HBI refinements.

For the present problem, one can eliminate the thermal penetration depth δ from Eqs. (24) and (25) to produce a single ODE in the primary unknown θ_w. For convenience, denote the integral on the left side of Eq. (25) by I. Then with $\theta = \theta_w\theta^*$ and $\mathrm{d}z = \delta \mathrm{d}z^*$, this I and Eq. (24) become

$$I \equiv \int_0^\infty \theta(z, t)\, \mathrm{d}z = \theta_w \delta I^*, \qquad I^* = \int_0^\infty \theta^*\, \mathrm{d}z^* \tag{27}$$

$$\dot{q}_{\text{net}} = (\alpha_w \theta_w/\delta)\dot{q}^*_{\text{net}}, \qquad \dot{q}^*_{\text{net}} = (-\mathrm{d}\theta^*/\mathrm{d}z^*)_{z^*=0+} \tag{28}$$

where I^* and $\dot{q}^*_{\text{net}}$ are dimensionless constants corresponding to the given profile shape. Eliminating δ between Eqs. (27) and (28) yields $I = I^*\dot{q}^*_{\text{net}}(\theta_w^2\alpha_w/\dot{q}_{\text{net}})$, which, when substituted into Eq. (25), produces the desired ODE in $\theta_w(t)$

$$\frac{\mathrm{d}}{\mathrm{d}t}\left(\frac{K^*\theta_w^2\alpha_w}{\dot{q}_{\text{net}}}\right) = \dot{q}_{\text{net}} - \theta_w\dot{s} \tag{29}$$

Here $K^* = I^*\dot{q}^*_{\text{net}}$ is a positive constant, and $\alpha_w = \alpha(\theta_w)$, $\dot{q}_{\text{net}} = \dot{q}_{\text{net}}(t, \theta_w)$, and $\dot{s} = \dot{s}(t, \theta_w)$ are known functions. Given a θ_w solution and associated $\dot{q}_{\text{net}}$, Eq. (28) determines δ.

Depending on the choice of assumed profile, thermal penetration depth δ acquires different meanings. For the exponential profile $\theta^*(z^*) = \exp(-z^*)$, heat density is $1/e$-th of its wall value at $z = \delta$; also, $K^* = 1$, $I^* = 1$, and $\dot{q}^*_{\text{net}} = 1$. For $\theta^*(z^*) = (1 - z^*)^n$, the polynomial profile, δ is the time-dependent depth beyond which the heat entering the slab surface has effectively not yet penetrated. Thus θ and $\partial\theta/\partial z$ are zero for $z \ge \delta$, and one can substitute δ for ∞ in Eqs. (25) and (27) [the right-most part of Eq. (27) then integrates from 0 to 1]. Also, $K^* = n/(n + 1)$, $I^* = 1/(n + 1)$, and $\dot{q}^*_{\text{net}} = n$, where again, n need not be an integer.

For illustration, the example below uses the exponential profile exclusively. In fact, the exponential profile also originates from a quasisteady solution[22] of Eq. (21), and it fits exact finite-difference solutions better in-depth than do polynomials for the present case.[21]

The simplest, most reliable way to solve Eq. (29) numerically is to integrate it with respect to time, apply the trapezoidal rule of integration, and solve the resulting implicit, nonlinear equation by bisection. Thus, Eq. (29) becomes

$$K^*\frac{\theta_w^2\alpha_w}{\dot{q}_{\text{net}}} = I^o + \left(\dot{q}^o_{\text{net}} - \theta^o_w\dot{s}^o\right)\left(\frac{\Delta t}{2}\right) + \left(\dot{q}_{\text{net}} - \theta_w\dot{s}\right)\left(\frac{\Delta t}{2}\right) \tag{30}$$

where o-superscripts denote known values from the "old" time point t^o, unsuperscripted variables are values at the new (current) time t, and $\Delta t = t - t^o$ is the time step. Since α_w, $\dot{q}_{\text{net}}$, and $\dot{s}$ are essentially known functions of θ_w at a given time point, Eq. (30) is an implicit, nonlinear equation in one unknown, θ_w. The iterative method of bisection solves the equation and is guaranteed to converge provided a solution for the current θ_w exists and can be bracketed. At worst, the values of θ corresponding to $T_w = 300$ K and 5000 K suffice to bracket the solution (if one exists) and start the bisection. Given a

converged θ_w solution at the current time, the α_w, $\dot{q}_{net}$, $\dot{s}$, s, I, and δ are updated, and another time step is taken.

Mathematical Requirements

Although bisection is guaranteed to converge under ordinary circumstances, it is possible for classical HBI to fail. Certain nonlinearities in heat loads and material properties preclude existence of a mathematical solution. Moreover, failure (of the type shown in Fig. 2 of Ref. 20) can occur without obvious violation of the physical assumptions behind HBI. Potts,[19–21] therefore, established sufficient conditions to guarantee existence and uniqueness. The conditions are as follows. The function $\alpha(\theta_w)$ must be strictly positive, bounded away from zero, and twice continuously differentiable; $\dot{q}_{net}(t, \theta_w)$ must be strictly positive, bounded above by a maximum, and twice continuously differentiable; $\dot{s}(t, \theta_w)$ must be non-negative and continuously differentiable; finally, for any fixed t, the combination of variables appearing on the left side of Eq. (29), call it $\Psi(t, \theta_w) \equiv \theta_w^2 \alpha(\theta_w)/\dot{q}_{net}(t, \theta_w)$, must be a strictly monotone increasing function of θ_w; i.e., $\partial\Psi/\partial\theta_w > 0$ for all $\theta_w > 0$.

Potts[19,20] originally expressed this last condition as two separate conditions, namely, $d[\theta_w^2\alpha(\theta_w)]/d\theta_w > 0$ and $\partial\dot{q}_{net}/\partial\theta_w \leq 0$. But the latter, which says $\dot{q}_{net}$ must never increase with θ_w at any fixed t, is violated by the $\dot{q}_{net}$ in this paper.

Ordinarily, the net heat transfer from a hot boundary layer into a wall decreases as the wall gets hotter. This is true for endothermic surface chemical reactions, positive heats of ablation, and nonreacting walls. But in the diffusion plateau, carbon oxidation is exothermic (note the drop in h_w around 1300 K in Fig. 3), and $\dot{q}_{net}$ increases briefly with increasing θ_w. Still, for the carbon-carbon model presented here, classical HBI does not fail, for the unified condition on $\Psi \equiv \theta_w^2\alpha_w/\dot{q}_{net}$ holds. The increase in the denominator, $\dot{q}_{net}$, in the oxidation onset regime is compensated by a greater increase in the numerator, $\theta_w^2\alpha(\theta_w)$, over this same regime, so that the ratio Ψ is strictly monotone increasing in θ_w for every fixed t.

Note that when $\dot{q}_{net}$ is constant, $\theta^2\alpha$ must still have a positive derivative, which limits the rate and extent to which an α function can decrease as θ increases. This is more than an academic matter, for note that the α for carbon-carbon decreases substantially with increasing temperature and θ (Table 1). Nonetheless, by avoiding an overly coarse $\alpha - \theta$ data table, or a poor $\alpha(\theta)$ curve fit, $\theta^2\alpha$ retains a strictly positive derivative.

For computer applications, strict adherence to continuous differentiability can often be relaxed. Computer codes often involve table interpolation. Since derivatives of α_w, $\dot{q}_{net}$, and $\dot{s}$ are not required in the numerical trapezoidal-bisection solution of Eq. (30), it suffices if α_w, $\dot{q}_{net}$, and $\dot{s}$ are continuous, piecewise linear. Violation of differentiability at the isolated segment "joints" is harmless, for in the subintervals, the required mathematical conditions apply. Overall continuity from one subinterval to the next then preserves the necessary "smoothness."[19,48]

Finally, note that $\dot{q}_{net}$ must stay positive in classical HBI. The $\theta - z$ profile requires a negative slope, which by Eq. (24) implies a positive $\dot{q}_{net}$. Physically $\dot{q}_{net}$ can become zero or negative, particularly in the final seconds of re-entry, when the RV has slowed down and the hot RV surface is giving up heat. For successful application of classical HBI, a positive lower bound must be imposed on $\dot{q}_{net}$. For predominantly hypersonic re-entry, a minute lower bound, such as 0.1 W/cm^2, which is orders of magnitude smaller than peak heating, suffices without harm.

The overall lesson is this. When a solution technique, such as classical HBI, employs assumptions that are physically reasonable but not always strictly correct, unexpected mathematical constraints may crop up (e.g., monotonicity of $\Psi \equiv \theta_w^2\alpha_w/\dot{q}_{net}$) along with the more obvious but also artificial physical constraints (e.g., $\dot{q}_{net} > 0$). Approximate solution techniques must always be checked mathematically for hidden, nonphysical failure modes. Refinements to classical HBI may require completely different constraints, but the techniques in Ref. 19 generally apply.

Illustrative Example

An example illustrates the performance of classical HBI for relatively realistic conditions. A blunt RV of high ballistic coefficient

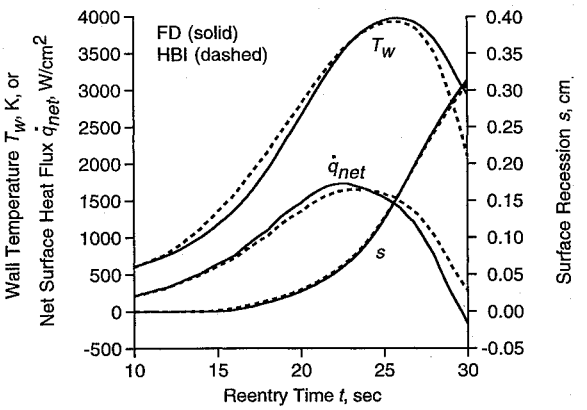

Fig. 4 Example comparison of finite-difference (FD) and classical heat balance integral (HBI) solutions.

(e.g., 2000 lbf/ft^2 or 95,760 N/m^2) traverses the earth's atmosphere from 90 km to sea-level in 30 seconds. The RV begins re-entry with speed 6000 m/s and, because of its large momentum and ballistic coefficient, travels roughly in a straight path, maintaining a re-entry angle of about −30 degrees from the horizontal. The nose tip is carbon-carbon with nose radius 5 cm.

Following loosely the analysis of Allen and Eggers,[49] the following functions approximate the local freestream density ρ_∞ and speed u_∞ encountered by the RV as a function of time t from start of re-entry: $\rho_\infty = (1.75 \times 10^{-3})t^*$ in g/cm^3 and $u_\infty = 6000\exp\{-1.2t^*\}$ in m/s, where $t^* = \exp\{(t - 30)/2.2\}$.

Stagnation point response is of interest. Hypersonic stagnation point pressure is approximately twice the freestream dynamic pressure and is non-dimensionalized in this paper so that it numerically equals the value in atmospheres, or approximately bars; thus, $P^* = (\rho_\infty u_\infty^2) \times 10^{-2}$. Recovery enthalpy is taken as total enthalpy for the stagnation point; thus $h_r = (u_\infty^2/2) \times 10^{-3}$ in J/g. Finally, akin to Ref. 49, stagnation point cold wall heating rate follows $\dot{q}_{cw} = 5 \times 10^{-6}(\rho_\infty/R_N)^{1/2}u_\infty^3$ in W/cm^2. For illustration, assume the nose tip maintains a constant radius $R_N = 5$ cm as it ablates in clear air.

For non-charring carbon-carbon, ρ is essentially constant (= 1.90 g/cm^3), so Eq. (20) becomes a constant factor of Eq. (7); i.e., $\theta = \rho h_u$. Since Eq. (13) and $\theta = \rho h_u$ use Eq. (7), Table 1 uses Eq. (6) for consistency to define α. Linear interpolation of the data values in Table 1 defines $\alpha(\theta)$. Alternatively, $\alpha(\theta) = 0.116 + 0.690\exp\{-\theta/(886 + 0.125\theta)\}$ in cm^2/s fits this brand of carbon-carbon. Note that this $\alpha(\theta)$ satisfies earlier mathematical requirements; e.g., $d[\theta^2\alpha(\theta)]/d\theta > 0$ for all $\theta > 0$.

Figure 4 shows good agreement between classical HBI and finite-difference calculations, which are taken as the standard. Run times for this clear-air case on a VAX 6540 are 10.25 CPU seconds for finite-difference and 1.13 CPU seconds for HBI. For typical erosion cases (not presented), classical HBI again agrees closely with finite-difference results and runs from 20 to 60 times faster on the VAX. Thus, HBI has significant advantages over more exact but slower finite-difference methods.

Pulse-Like Heat Loads

The rising then plummeting $\dot{q}_{net}$ in Fig. 4 falls under the class of "pulselike inputs,"[12] and here Fig. 4 displays a common problem of classical HBI: it overreacts to rapidly changing heat loads. Surface temperature is overpredicted when heating rates are rising rapidly and underpredicted, sometimes significantly, when heating rates are falling rapidly. The prediction stays poor during most of a protracted period of low heating following a peak, and this spoils HBI's in-depth temperature. From Eq. (27), an underpredicted θ_w implies an overpredicted δ for the same I, and hence an overpredicted in-depth temperature. The problem is the instantaneous effect of net heat flux on the wall slope and thermal penetration depth of the in-depth profile. Refinements to classical HBI by Goodman,[12] Zien,[16,17] and Leone et al.[23,24] may relieve this "slope effect" (overreaction problem) somewhat.

Goodman's extended method[12] decomposes the solution following the net heat flux peak into two fictitious parts. The first part continues propagation of the thermal penetration distance, but with net heat flux frozen at its peak value. The second part propagates a thermal cooling distance using a negative net heat flux equal to the difference between the actual net heat flux and the peak net heat flux. This negative net heat flux is applied to a fictitious slab whose initial temperature, at the time of peak heating, is uniform at all points in-depth and equals the peak wall temperature of the real slab. This second penetration distance accounts for the change in curvature of the in-depth thermal profile during cool down.

Two problems limit use of Goodman's extended method. First, differing onset times of ablation, charring, pyrolysis outgassing, and intermittent erosion may produce a $\dot{q}_{\text{net}}$ history with multiple peaks, which are hard to locate in advance. This presents at least a bookkeeping problem if not worse in the algorithm. Second, closed-form solution of Goodman's extended method requires constant material properties; in fact, superposition of solutions works best for simple linear problems, not the nonlinear complexities here.

The moment methods of Zien[16,17] may avoid both overreaction and unexpected failure problems. In both classical and Zien's integral methods, Eq. (25) is the primary equation, as obtained by one spatial integration of Eq. (21), and a profile shape for the heat distribution is assumed. In classical HBI, the second equation is Eq. (24), so there are two equations in the two unknowns δ and θ_w. In Zien's θ-moment method, however, the second equation is obtained by multiplying Eq. (21) by θ, integrating it spatially, using integration by parts and the Leibnitz rule, and applying the boundary conditions to produce

$$\frac{1}{2}\frac{\mathrm{d}}{\mathrm{d}t}\int_0^\infty \theta^2\,\mathrm{d}z = \theta_w\dot{q}_{\text{net}} - \int_0^\infty \alpha(\theta)\left(\frac{\partial\theta}{\partial z}\right)^2\mathrm{d}z - \frac{\dot{s}}{2}\theta_w^2 \qquad (31)$$

In Zien's z-moment method, Eq. (21) is multiplied by z, integrated spatially, etc., to produce

$$\frac{\mathrm{d}}{\mathrm{d}t}\int_0^\infty z\theta\mathrm{d}z = -\int_0^\infty \alpha(\theta)\frac{\partial\theta}{\partial z}\,\mathrm{d}z - \dot{s}\int_0^\infty \theta\,\mathrm{d}z \qquad (32)$$

Equation (32) can also be derived[16] by performing a double spatial integration of Eq. (21). In either case, the assumed temperature or heat distribution profile, Eq. (26), is applied to Eqs. (31) or (32), resulting in a second equation involving θ_w, δ, $\dot{\theta}_w$, and $\dot{\delta}$. The system of two equations can be re-expressed in the form $\dot{\theta}_w = f_1(\theta_w, \delta, \ldots)$ and $\dot{\delta} = f_2(\theta_w, \delta, \ldots)$ [see, for example, Eqs. (18–20) of Chung and Hsiao[17]], and then standard numerical techniques for solving a system of two or more ODEs can be employed.

An advantage of Zien's methods is that they weaken the sensitivity of the integral solution to the instantaneous $\dot{q}_{\text{net}}$. Instead of determining the profile slope by $\dot{q}_{\text{net}}$ per Eq. (24) as in classical HBI, the profile shape is determined by an integral moment. Thus, Zien's methods are less apt to overreact to sudden changes in heat load or to the decreasing side of a heat pulse. Moreover, the restriction $\mathrm{d}[\theta^2\alpha(\theta)]/\mathrm{d}\theta > 0$ may be unnecessary for Zien's methods; specific domains of validity have not yet been delineated using the methods in Ref. 19.

An inconvenience of Zien's methods concerns the α-integrals on the right sides of either Eq. (31) or (32). For non-constant α functions, these α-integrals must be evaluated numerically as functions of θ_w and stored tabularly ahead of time. Also, Zien's methods have not been extended to charring ablator problems.

Leone et al.[23,24] treat the HBI overreaction problem in a manner reminiscent of Goodman's fictitious slab technique. The net heat flux determines the instantaneous profile slope at the wall, but, unlike classical HBI, it does not affect the thermal penetration depth δ. Instead, an independent $\delta(t)$ history is assumed. That way, the profile near the wall can take on any slope according to a positive, zero, or negative net heat flux. For nonpositive $\dot{q}_{\text{net}}$, a "generalized cubic" profile is used to allow for the appropriate change in curvature. Details are available in Ref. 24. Presumption of a presupposed $\delta(t)$ history may be open to objection but seems to work in practice. Leone's method has also been extended to charring ablators.[23,24]

Charring Ablators

To apply HBI to charring ablators, one must decide 1) how to set up the in-depth profiles for the unknown variables, T, ρ, and $\dot{m}_g$, and 2) whether or to what extent should these profiles be coupled to each other and stay coupled to the governing equations to effect an efficient, accurate solution while avoiding numerical instabilities. For reliability, any simplifications and idealizations that modify the couplings (i.e., governing equations) should also find physical justification.

Most HBI approaches use step functions for the ρ and $\dot{m}_g$ profiles.[13,21–24] The resin decomposition zone is generally so thin[7,15,21–24] that the in-depth region effectively divides into virgin and fully-charred regions, as demarcated by an effective char depth δ_c. Therefore, $\rho = \rho_c$ and $\dot{m}_g = \dot{m}_{gw}$ for $0 < z < \delta_c$, and $\rho = \rho_v$ and $\dot{m}_g = 0$ for $\delta_c < z < \delta$.

Following Adarkar and Hartsook,[13] the ρ and $\dot{m}_g$ are related by conservation of mass:

$$\dot{m}_{gw} = (\dot{s} + \dot{\delta}_c)(\rho_v - \rho_c) \qquad (33)$$

More formally, spatial integration of Eq. (23) produces Eq. (33), where, for ρ a step function, $\partial\rho/\partial t$ in Eq. (23) becomes a Dirac delta functional or impulse function. The substitution $\mathrm{d}z = \dot{\delta}_c\,\mathrm{d}t$ permits integration of this term.

Since the ρ and $\dot{m}_g$ profiles follow a two-layer approach, a two-layer approach for T might at first seem logical. An example would be $T = T_w[1 - z/\delta_c] + T_c[z/\delta_c]$ for $0 < z < \delta_c$ and $T = T_c[1 - (z - \delta_c)/(\delta - \delta_c)]^n$ for $\delta_c < z < \delta$. Here T_c represents a known, fixed char temperature.[13] Equation (1) applies across the virgin layer, and Eq. (2) with the $\Delta h_{\text{pyr}(g)}$ term discarded applies across the char layer.[13] Across the char front

$$\left(-k_c\frac{\partial T}{\partial z}\right)_{z=\delta_c-} - \dot{m}_{gw}\Delta h_{\text{pyr}(g)} = \left(-k_v\frac{\partial T}{\partial z}\right)_{z=\delta_c+} \qquad (34)$$

as derived in Refs. 13 and 22 [see Eq. (54b)]. At the surface, Eqs. (5) and (10–13) apply. Application of the two-layer T profile to Eqs. (1), (2), (5), and (34) produces a complex system of equations involving T_w, δ, δ_c, $\dot{m}_{gw}$, and $\dot{q}_{\text{net}}$. And these are also coupled with Eqs. (10–13) and (33).

For a simple melt-removal ablation model without complex blowing, the above complex system apparently succeeds.[13] But for the complex ablation, blowing, and energy balance of the present paper, an oscillatory feedback erupts among $\dot{q}_{\text{net}}$, $\dot{m}_{gw}$, and $\dot{\delta}_c$ at some point, and insurmountable numerical instabilities result.[22] Somehow, this total two-layer approach is too complex and too closely coupled.

To cut down on the number of profile parameters, and, therefore, coupled equations and potential instabilities, most charring HBI methods use a one-layer approach for the T profile, while maintaining the two-layer approach for the ρ and $\dot{m}_{gw}$ profiles. To make this possible, a $\rho(T)$ relationship must be assumed. Since virgin property measurements are generally available only in the low temperature regime, and char property measurements only in the high temperature regime (Fig. 2), there is a natural association $\rho = \rho(T)$ in the data to begin with (Table 2). Assumption of a $\rho = \rho(T)$ is common practice[3,14,15,21,22,28] and permits use of Eqs. (20) and (22).

With Eqs. (21), (25), and (27) in mind, spatial integration of Eq. (22) produces[22]

$$\dot{I} = \dot{q}_{\text{net}} - \theta_w\dot{s} - \dot{m}_{gw}\Delta h_{\text{pyr}(g)} - \dot{m}_{gw}c_{\text{pg}}(T_w - T_c) \qquad (35)$$

The $\Delta h_{\text{pyr}(g)}$ term integrates as above under the assumption that either $\Delta h_{\text{pyr}(g)}$ is constant or $\dot{m}_g$ takes a step-function profile, implying $\partial\dot{m}_g/\partial z$ is a Dirac delta functional. The final term integrates assuming both c_{pg} is constant and $\dot{m}_g$ is a step function, so that $\dot{m}_g c_{\text{pg}}$ is constant except for the step jump at the char front.

Early one-layer HBI approaches[14,15,21] neglected the two final terms of Eq. (22) and often resorted to correlations. Another try puts a finite spike in the $c_p(T)$ function to model the heat absorbed in the in-depth charring reaction (see Ref. 28, Fig. 2, p. 176). This device may work for finite-difference and finite-element methods, but not in general for classical HBI methods, because it risks violating the condition that $\theta^2\alpha(\theta)$ have a positive derivative. (The situation is

complex because α decreases but θ increases when c_p increases.) In any case, Eq. (35) sidesteps these problems.

To use Eq. (35), solutions for $\dot{m}_{gw}$, T_c, and δ_c must be obtained. Potts[22] and Leone et al.[23,24] offer two approaches.

First, Potts obtains T_c as a known constant. The coefficients in Eq. (4) usually stem from experiments conducted at specific temperature rise rates.[2,22,34] Hypothesize an operative rise rate, such as 1000 K/sec for clear-air re-entry, and solve Eq. (4) in stand-alone fashion. The 50% char point yields an effective char temperature T_c. Finite-difference solutions of Eqs. (2–4) may also be examined. For the coefficients in Ref. 7, typical values are 1000 K and 1450 K for the 5 and 50% points of char in pure ablation (clear-air) cases, and 1250 K and 1800 K for 5 and 50% points of char in coupled ablation-erosion situations.[21,22,24] The chosen T_c may disagree with the assumed $\rho(T)$ in Table 2 and Eq. (20), but this intentionally decouples the problem further and avoids numerical instabilities. Global (integral) energy is still conserved despite any ambiguity about where charring takes place in-depth.

Next, Potts obtains δ_c by assuming a linear thermal profile across the char layer. First, approximate Eq. (24) by $\dot{q}_{\text{net}} = \alpha_w(\theta_w - \theta_c)/\delta_c$, where Eq. (20) relates T_c to θ_c. Then solve for δ_c given θ_w and $\dot{q}_{\text{net}}$; i.e.,

$$\delta_c = \max\left\{\alpha_w(\theta_w - \theta_c)/\dot{q}_{\text{net}}, \quad \delta_c^o - (\dot{s} + \dot{s}^o)\Delta t/2, \quad 0\right\} \tag{36}$$

The added terms in Eq. (36) prevent δ_c from decreasing faster than the surface recession or from becoming negative. This prevents the unphysical phenomenon of "de-charring," in which charred material becomes virgin again merely by cooling to below T_c.

Finally, Potts obtains $\dot{m}_{gw}$ by employing the "quasisteady state" concept.[6,22] Quasi-steady state means that changes in the temperature and density distribution in the material, as measured from the moving surface, are small with respect to time. Quasi-steady solutions, therefore, are obtained by transforming the governing equations to a coordinate system moving with the surface, and then casting out all the time derivatives of the dependent variables while still allowing the boundary conditions to vary with time.

Under a quasisteady assumption, $\dot{I}$ and $\partial\rho/\partial t$ are temporarily set to zero. Spatial integration of Eq. (23) with $\partial\rho/\partial t = 0$ produces $\dot{m}_{gw} = \dot{s}(\rho_v - \rho_w)$, which is used to replace $\dot{s}$ temporarily in Eq. (35). With $\dot{I}$ also temporarily set to zero, the modified Eq. (35) produces

$$\dot{m}_{gw} = \dot{q}_{\text{net}}/[\theta_w/(\rho_v - \rho_w) + \Delta h_{\text{pyr}(g)} + c_{\text{pg}}(T_w - T_c)] \tag{37}$$

The elimination of $\dot{s}$ makes Eq. (37) produce reasonable gas fluxes even when the material undergoes non-quasisteady response. The $\rho_w(T)$ function in Eq. (37) and the $\rho(T)$ in Eq. (20) are separate in general: the $\rho_w(T)$ is tailored to produce a continuous transition from ρ_v to ρ_c around T_c; the $\rho(T)$ follows Table 2. The full HBI of Eq. (35), with $\dot{s}$ included and $\dot{I}$ no longer set zero, then is the fundamental energy equation, and Eq. (37) provides $\dot{m}_{gw}$.

Potts's hybrid integral-quasisteady approach, Eqs. (35–37) with specified T_c, proves to be fast and reasonably accurate.[22,24] Ref. 22 also presents a purely quasisteady solution of Eqs. (2–4) and shows that this solution fails to achieve the required accuracy for $\dot{m}_{gw}$ and δ_c. But most recently an alternative HBI approach was developed by Leone et al.[23,24] to incorporate Eq. (4) more directly and eliminate the necessity of developing a constant, effective T_c. Basically, Leone assumes $\rho = \rho_v$ in Eq. (4), making the char rate a function of temperature alone. Then with a suitably simple temperature profile, Eqs. (3) and (4) are integrated spatially to produce $\dot{m}_{gw}$ as a function of temperature at the char depth. Using this variable char temperature from the previous time point, motion of the char front derives from Eq. (33). Ordinarily, such a procedure might be numerically unstable because of the overreaction of HBI to rapid changes in heat load. But Leone's non-classical generalized cubic method, discussed earlier, diminishes this overreaction, so is an essential part of the success of his approach to charring. Typical run times for Potts's HBI,[22] Leone's HBI,[23,24] and finite-difference[7] solutions are 4, 15, and 50 seconds, respectively, on a VAX 6440. These and numerical comparisons are shown in Ref. 24. Results show that temperature at the char front usually holds constant.

IV. Conclusions

1) Approximate HBI methods offer speed, simplicity, and versatility. For many applications, they provide sufficient accuracy.

2) For non-charring, primarily hypersonic re-entry, classical HBI works well.

3) If overreaction of classical HBI to cool down becomes significant, HBI extensions can be tried. Goodman's extended method treats simple linear problems. Zien's methods apply to non-charring, nonlinear problems. Leone's method treats nonlinear problems with charring. If these fail to satisfy a user's accuracy requirements, one must revert to finite-difference and pay the computational cost.

4) For charring ablation simulations, HBI methods require simplifying assumptions, particularly to form a pre-solution relationship between material density and temperature.

5) For quick simulation of charring in hypersonic flow, the hybrid integral-quasisteady approach of Potts is recommended. As computational speed becomes less important and accuracy away from peak heat or environmental loads becomes more important, the recommendation shifts towards Leone's method, or else finite-difference. For simplified ablation and energy balance models, Adarkar and Hartsook's approach can be tried.

References

[1]Sutton, G. W., "The Initial Development of Ablation Heat Protection, An Historical Perspective," *Journal of Spacecraft and Rockets*, Vol. 19, No. 1, 1982, pp. 3–11.

[2]Shaw, T. E., Garner, D. C., and Florence, D. E., "Effects of Uncertainties in Thermophysical Properties on Ablation Efficiency," *Thermophysics and Temperature Control of Spacecraft and Entry Vehicles*, edited by G. B. Heller, Vol. 18, Progress in Astronautics and Aeronautics, Academic Press, New York, 1966, pp. 513–548.

[3]Moyer, C. B., and Rindal, R. A., "An Analysis of the Coupled Chemically Reacting Boundary Layer and Charring Ablator, Part II, Finite Difference Solution for the In-Depth Response of Charring Materials Considering Surface Chemical and Energy Balances," NASA CR-1061, June 1968.

[4]Schneider, P. J., Dolton, T. A., and Reed, G. W., "Mechanical Erosion of Charring Ablators in Ground-Test and Re-Entry Environments," *AIAA Journal*, Vol. 6, No. 1, 1968, pp. 64–72.

[5]Lorenz, G. C., "Simulation of the Erosive Effects of Multiple Particle Impacts in Hypersonic Flow," *Journal of Spacecraft and Rockets*, Vol. 7, No. 2, 1970, pp. 119–125.

[6]Quan, V., "Quasi-Steady Solution for Ablation-Erosion Heat Transfer," *Journal of Spacecraft and Rockets*, Vol. 7, No. 3, 1970, pp. 355–357.

[7]Clever, R. M., and Denny, V. E., "Response of Charring Ablators to Severe Aerodynamic and Erosion Environments," *Journal of Spacecraft and Rockets*, Vol. 12, No. 9, 1975, pp. 558–564.

[8]McMillen, L. D., Dunbar, L. E., and Jackson, D., "Heatshield Materials Erosion at Hypersonic Velocities," AIAA Paper 76-321, July 1976.

[9]Papadopoulos, P., Tauber, M. E., and Chang, I.-D., "Heatshield Erosion in a Dusty Martian Atmosphere," *Journal of Spacecraft and Rockets*, Vol. 30, No. 2, 1993, pp. 140–151.

[10]Milos, F. S., and Rasky, D. J., "Review of Numerical Procedures for Computational Surface Thermochemistry," *Journal of Thermophysics and Heat Transfer*, Vol. 8, No. 1, 1994, pp. 24–34.

[11]Moulton, J. F., Jr., "Re-entry Vehicle Fratricide Constraints on Attack Planning," Defense Nuclear Agency, DNA 5012D, Washington, DC, Jan. 1978.

[12]Goodman, T. R., "Application of Integral Methods to Transient Nonlinear Heat Transfer," *Advances in Heat Transfer*, Vol. I, edited by T. F. Irvine and J. P. Hartnett, Academic Press, New York, 1964, pp. 51–122.

[13]Adarkar, D. B., and Hartsook, L. B., "An Integral Approach to Transient Charring Ablator Problems," *AIAA Journal*, Vol. 4, No. 12, 1966, pp. 2246–2248.

[14]Quan, V., "Integral Solution for Erosion Heat Transfer," *AIAA Journal*, Vol. 8, No. 8, 1970, pp. 1512–1514.

[15]Laganelli, A. L., Harper, T. P., and Fogaroli, R. P., "Integral Solution for Thermal Performance of a Charring Ablator," *Heat Transfer with Thermal Control Applications*, edited by M. M. Yovanovich, Vol. 39, Progress in Astronautics and Aeronautics, AIAA and The MIT Press, Cambridge, MA, 1975, pp. 375–393.

[16]Zien, T. F., "Study of Heat Conduction with Phase Transition Using an Integral Method," *Thermophysics of Spacecraft and Outer Planet Entry Probes*, edited by A. M. Smith, Vol. 56, Progress in Astronautics and Aeronautics, AIAA, New York, 1977, pp. 87–111.

[17]Chung, B. T. F., and Hsiao, J. S., "Heat Transfer with Ablation in a Finite Slab Subjected to Time-Variant Heat Fluxes," *AIAA Journal*, Vol. 23,

No. 1, 1985, pp. 145–150.

[18]Bell, G. E., and Abbas, S. K., "Convergence Properties of the Heat Balance Integral Method," *Numerical Heat Transfer*, Vol. 8, No. 3, 1985, pp. 373–382.

[19]Potts, R. L., "Analysis of an Integral Method for Computing Re-entry Vehicle Heat Conduction in Systems Level Computer Codes," AIAA Paper 81-0283, Jan. 1981.

[20]Potts, R. L., "An Integral Method Theorem for Heat Conduction," *AIAA Journal*, Vol. 21, No. 4, 1983, pp. 630, 631.

[21]Potts, R. L., "On Heat Balance Integral Solutions of Carbonaceous Ablator Response During Re-entry," AIAA Paper 84-0393, Jan. 1984.

[22]Potts, R. L., "Hybrid Integral/Quasi-Steady Solution of Charring Ablation," AIAA Paper 90-1677, June 1990.

[23]Leone, S. A., and Laganelli, A. L., "Enhancements to Approximate Ablation Techniques," AIAA Paper 92-0854, Jan. 1992.

[24]Leone, S. A., Potts, R. L., and Laganelli, A. L., "Enhancements to Integral Solutions to Ablation and Charring," *Journal of Spacecraft and Rockets*, Vol. 32, No. 2, 1995, pp. 210–216.

[25]Kendall, R. M., Rindal, R. A., and Bartlett, E. P., "A Multicomponent Boundary Layer Chemically Coupled to an Ablating Surface," *AIAA Journal*, Vol. 5, No. 6, 1967, pp. 1063–1071.

[26]Wenger, R. S., Laganelli, A. L., and Somers, J., "Nuclear Radiation Effects on the Ablation Performance of Advanced Composite Heatshield Materials," AIAA Paper 81-1059, June 1981.

[27]Bueche, J. F., "Effects of Improvements and Uncertainties in Thermophysical Properties on Carbon Phenolic Heatshield Thermal Performance Predictions," AIAA Paper 77-787, June 1977.

[28]Chang, C. I., Griffis, C. A., Stonesifer, F. R., and Nemes, J. A., "Thermomechanical Effects of Intense Thermal Heating on Materials /Structures," *Journal of Thermophysics and Heat Transfer*, Vol. 1, No. 2, 1987, pp. 175–181.

[29]Taylor, R. E., Groot, H., and Shoemaker, R. L., "Thermophysical Properties of Fine Weave Carbon/Carbon Composites," *Spacecraft Radiative Transfer and Temperature Control*, edited by T. E. Horton, Vol. 83, Progress in Astronautics and Aeronautics, AIAA, New York, 1982, pp. 96–108.

[30]Wakefield, R. M., and Peterson, D. L., "Graphite Ablation in Combined Convective and Radiative Heating," *Journal of Spacecraft and Rockets*, Vol. 10, No. 2, 1973, pp. 149–154.

[31]Park, C., "Stagnation-Point Ablation of Carbonaceous Flat Disks—Part I: Theory," *AIAA Journal*, Vol. 21, No. 11, 1983, pp. 1588–1594.

[32]Stull, D. R., et al., *JANAF Thermochemical Tables*, 2nd ed., Dow Chemical Company and U.S. Department of Commerce, National Bureau of Standards, NSRDS-NBS 37, Washington, D. C., June 1971.

[33]Cezairliyan, A., and Miiller, A. P., "Specific Heat Capacity and Electrical Resistivity of a Carbon-Carbon Composite in the Range 1500–3000 K by a Pulse Heating Method," *International Journal of Thermophysics*, Vol. 1, No. 3, 1980, pp. 317–330.

[34]Auerbach, I., Benson, D. A., Beard, S. G., and Wright, G. F., Jr., "Evaluation of Thermal and Kinetic Properties Suitable for High Heating Rate Computations," *Journal of Thermophysics and Heat Transfer*, Vol. 3, No. 4, 1989, pp. 395–400.

[35]Mills, A. F., "Convective Heat and Mass Transfer to Re-entry Vehicles," School of Engineering and Applied Science, University of California, Los Angeles, UCLA-ENG-7892, Los Angeles, CA, Dec. 1978.

[36]Mills, A. F., and Wortman, A. "Two-Dimensional Stagnation Point Flows of Binary Mixtures," *International Journal of Heat and Mass Transfer*, Vol. 15, No. 5, 1972, pp. 969–987.

[37]Putz, K. E., and Bartlett, E. P., "Heat-Transfer and Ablation-Rate Correlations for Re-Entry Heat-Shield and Nosetip Applications," *Journal of Spacecraft and Rockets*, Vol. 10, No. 1, 1973, pp. 15–22.

[38]Hove, D. T., and Shih, W. C. L., "Re-Entry Vehicle Stagnation Region Heat-Transfer in Particle Environments," *AIAA Journal*, Vol. 15, No. 7, 1977, pp. 1002–1005.

[39]Scala, S. M., and Gilbert, L. M., "Sublimation of Graphite at Hypersonic Speeds," *AIAA Journal*, Vol. 3, No. 9, 1965, pp. 1635–1644.

[40]Powars, C. A., and Kendall, R. M., "User's Manual, Aerotherm Chemical Equilibrium (ACE) Computer Program," Aerotherm Corporation, UM-69-7, Mountain View, CA, May 1969.

[41]Baker, R. L., and Covington, M. A., "The High Temperature Thermochemical Properties of Carbon," The Aerospace Corporation, SD-TR-82-19, El Segundo, CA, March 1982.

[42]Metzger, J. W., Engel, M. J., and Diaconis, N. S., "Oxidation and Sublimation of Graphite in Simulated Re-Entry Environments," *AIAA Journal*, Vol. 5, No. 3, 1967, pp. 451–460.

[43]Hunter, L. W., Perini, L. L., Conn, D. W., and Brenza, P. T., "Calculation of Carbon Ablation on a Re-Entry Body During Supersonic/Subsonic Flight," *Journal of Spacecraft and Rockets*, Vol. 23, No. 5, 1986, pp. 487–491.

[44]Swain, C. E., "The Effect of Particle/Shock Layer Interaction on Re-entry Vehicle Performance," AIAA Paper 75–734, May 1975.

[45]Reinecke, W. G., "Debris Shielding during High-Speed Erosion," *AIAA Journal*, Vol. 12, No. 11, 1974, pp. 1592–1594.

[46]Waldman, G. D., and Reinecke, W. G., "Particle Trajectories, Heating, and Breakup in Hypersonic Shock Layers," *AIAA Journal*, Vol. 9, No. 6, 1971, pp. 1040–1048.

[47]Park, C., "Stagnation-Point Ablation of Carbonaceous Flat Disks—Part II: Experiment," *AIAA Journal*, Vol. 21, No. 12, 1983, pp. 1748–1754.

[48]Shampine, L. F., and Allen, R. C., Jr., *Numerical Computing: An Introduction*, Saunders, Philadelphia, 1973, p. 137.

[49]Allen, H. J., and Eggers, A. J., Jr., "A Study of the Motion and Aerodynamic Heating of Ballistic Missiles Entering the Earth's Atmosphere at High Supersonic Speeds," NACA Report 1381, 1958.

T. C. Lin
Associate Editor